Egyptian Journal of Chemistry

http://ejchem.journals.ekb.eg/

Boosting the sunlight irradiation and methylene blue dye degradation over ZnO doped with N and C elements

Salma Fathya, Sahar Mousa[b], Nady Fathy[c]*, Farag Ali[a]

a) Department of Chemistry, Faculty of Science, Menoufia University, Menoufia, Egypt
b)Inorganic Chemistry Department, National Research Centre, 33 El Bohouth Street (former Tahrirst.), Dokki, Giza, P.O. 12622, Egypt.
c) Physical Chemistry Department, National Research Centre, 33 El Bohouth Street (former Tahrirst.), Dokki, Giza, P.O. 12622, Egypt..

Abstract

This article aims at preparing ZnO nanoparticles and doping with nitrogen (N) and carbon (C) nonmetals via sol-gel method followed by the calcination in N_2 and air media to mitigate the fast electron-hole pairs recombination drawbacks and improve the visible light photocatalytic activity of pure ZnO under sunlight irradiation. The influence of dopant content of N- and C-N doped ZnO on the photodegradation of methylene blue (MB) dye was investigated. To compare doped samples properties with ZnO bare, techniques such as X-ray diffraction (XRD), scanning electron microscope (SEM), energy-dispersive X-ray spectroscopy (EDX), fourier transform infrared (FTIR), Brunauer, Emmett and Teller (BET) surface area, and UV-Vis diffuse reflectance spectroscopy (DRS) were employed. Wurtize hexagonal structure of ZnO with good crystallinity of nanoparticles (NPs) ranged between 15.5 and 45.8 nm was confirmed by XRD. However, entering N into ZnO lattice decreased the crystallite size whereas doping with C-N enhanced the crystallite size of ZnO. Through SEM, ZnO NPs appeared as spherical morphology and FTIR showed the characteristic absorption bands related to Zn–O stretching and bending vibration modes with symmetric stretching vibration of O–C=O and–C–O groups were detected in FTIR. The bandgap value of ZnO was decreased from 3.07eV to 2.83eV upon doping with 40%N/ZnO(air). Pure ZnO exhibited 100% degradation of MB at 180 min, and ZnO doped with the highest concentrations of N and C-N dopants showed a full degradation of MB dye at 60 and 90 min, respectively. Thereof, the 40% N/ ZnO(air) material exhibited the higher visible-light activity compared with 40%C-N/ZnO(N_2), where a complete photodegradation of MB dye was obtained at 60min.This superior photoactivity for 40%N/ZnO catalyst is due to their capability in reducing the electron–hole pair recombination arising from its smaller bandgap energy value.

Keywords: ZnO nanoparticles, sol-gel method, doping, photocatalytic activity, sunlight irradiation.

1. Introduction

Wastewater system remediation technology provides a vital service to society and reduces its susceptibility to the effects of climate change. The ecosystem, animals, and people today are seriously harmed by the introduction of various pollutants into water resources, such as bacteria, heavy metal ions, and organic pollutants [1]. Among water pollutants, Dyes are a significant category of water pollutants released to wastewater through dye, textile, and other industrial operations. Unfortunately, the amount of dyes created in the world is believed to be over 100000 tones/year, with approximately 100 000 commercially available dyes manufactured each year being discharged into waste streams [2, 3]. Organic dyes from industrial waste, like many other organic pollutants, are a serious issue because of their high toxicity to aquatic creatures, which can have serious consequences for human health, plants, and aquatics. The majority of dye effluents (54%) released into the environment come from the textile sector, which is also responsible for more than half of all dye effluents currently found in the environment. The dyeing industry (21%), paper and pulp industry (10%), tannery and paint industry (8%), and dye manufacturing industry (7%), all generate significant amounts of dye effluent from various associated processes [4]. Because dyes have dangerous effects on human health and the ecosystem, dyes must be removed from wastewater before it is released into water resources. As a result, it is critical to find simple and low-cost methods and technologies for removing dyes from different wastewater sources.

*Corresponding author e-mail: fathyna.77@hotmail.com.; (Nady Fathy).
Receive Date: 09 April 2023, Revise Date: 04 May 2023, Accept Date: 21 May 2023
DOI: 10.21608/EJCHEM.2023.205080.7843

In order to eliminate dyes from wastewater, a variety of treatment techniques have been used over the years [2,3], including coagulation, advanced oxidation, adsorption, membrane separation, etc. Of these methods, Adsorption and photocatalysis technologies are believed to be effective techniques that have been the focus of many researchers [1, 3]. To prevent secondary pollution to the environment, combining both techniques by using materials with adsorption and photocatalytic properties would improve and lower the cost of treatment [5].

Photocatalytic oxidation of dye contaminants in industrial wastewater using semiconducting oxides could be a substitute for traditional techniques for enhancing the removal of wastewater. It has several benefits, including ease of use, high efficiency, lower energy consumption of energy, and limited secondary pollution. It enables green mineralization of organic pollutants due to its mild working conditions and ability to be powered by sunlight [5]. A number of substances have been used as photocatalysts for the degradation of environmental contaminants, including ZnO [6], CdS [7], Fe_2O_3 [8], WO_3 [9], TiO_2 [10], etc. On the other hand, such catalysts have problems such as high recombination efficiency of photo-generated electron-hole pairs, low visible-light absorption, and ease of aggregation [1]. Due to its high natural abundance, appropriate redox potential, non-toxicity, high photosensitivity, and low cost, ZnO has been shown to be a suitable alternative to TiO_2 for photocatalytic applications [10]. Because they have a significantly higher band gap of 3.2 eV, their ability to absorb light in the UV spectrum is limited. Furthermore, ZnO nanostructures are readily synthesized in a variety of morphologies but have a high energy bandgap [10-12]. As a result, numerous techniques for modifying the band gap of ZnO photocatalysts to prevent fast recombination and increase visible light absorption have been developed. Recently, for example, precious metal deposition [13], carrier load [15], composite semiconductor [14], doping metal ions [16, 17], and non-metallic doping [18-25] have been used to modify ZnO. According to research for doping ZnO with nonmetals such as C, N, and S, the photocatalytic activity of ZnO was significantly increased, with band gap energy lower than that of pure ZnO and thus a remarkable increase in the visible light absorption.

To synthesize nonmetal-doped ZnO, many methods have been devised, including the sol-gel process [26], hydrothermal process [27], wet chemical process [28], chemical vapor deposition [29], mechanochemical process [30], and high-energy milling [31]. Furthermore, the generation of ZnO nanoparticles by doping with N and/or C using a simple process such as sol-gel can produce a novel and high-yield product for use in methylene blue dye photocatalysis.

The major objective of this paper is to synthesize N and C-N co-doped ZnO through a sol-gel procedure. Different weight percentages of urea have been used as an organic source for both C and N dopants and annealed at 500ºC for 2h under an atmosphere of N_2 gas or air. Furthermore, the photocatalytic ability of N and C-doped either by mono-or co-doing of ZnO samples obtained through calcination at air or nitrogen at 500ºC for 2 h was evaluated for the breakdown of methylene blue (MB) from aqueous solutions under sunlight irradiation.

2. Experimental

2.1. Materials

The chemicals used were zinc acetate anhydrous ($Zn(CH_3COO)_2$, ADWIC Co.), ammonium hydroxide (NH_4OH, 33%, ADWIC Co.), urea (H_4N_2CO,ADWIC Co.), methylene blue ($C_{16}H_{18}ClN_3S$, Sigma-Aldrich Co.).

2.2. Synthesis of Pure ZnO

Zinc oxide (ZnO) nanoparticles sample was prepared by sol-gel method. In typical, zinc acetate solution (0.1M) was prepared using distilled water then ammonium hydroxide (NH_4OH, 33%) was added into the zinc solution dropwise under stirring until the pH becomes 8±0.5 to form a milky white gel. The gel was vigorously stirred (750 rpm) at 50 °C for 1 h. For ageing the formed gel, the precipitate was allowed to settle for overnight then filtered and washed with distilled water for several times to remove the residual impurities. The washed gel was dried at 80 °C for 2h and calcined at 500 °C for 2 h in air muffle furnace with heating rate of 10 °C min^{-1}.

2.3. Synthesis of ZnO doped with N and/or C

The doped ZnO with C and N materials were prepared according to the above-mentioned procedure of pure ZnO as explained in (2.2). Urea used as a source of both carbon and nitrogen elements; was added with different weight percents of 5, 15, 25 and 40 wt%. For co-doping ZnO with nitrogen-carbon, the formed gel was calcined in a tubular furnace (home-made stainless steel tube 2.5cmx50cm) under nitrogen flow (20 mL/min). For doping ZnO with nitrogen, the gel sample was calcined in air muffle furnace. The resulting photocatalyst samples were notified as xN/ZnO (air) and xC-N/ZnO (N_2), where x refers to weight percent of urea used (5 – 40 %), C-N is attributed to urea modifier and the calcination in presence of air or nitrogen, respectively. Finally, about eight modified ZnO samples were prepared beside bare sample, so the following physico-chemical characterizations were carried out for the sample

doped with 40wt% of urea as a representative example.

2.4. Materials characterization

2.4.1. X-ray diffraction spectroscopy

The X-ray diffraction (XRD) patterns were measured on a D8 advance diffractometer with Cu K α radiation (λ= 1.5418 Å) (Bruker, Karlsruhe, Germany). The average crystallite size of ZnO and their doped samples was calculated by the Debye–Scherrer equation:

$$D_{khl} = K\lambda/\beta_{khl}\cos\theta \quad (1)$$

Where, D_{khl} is the crystallite size of (*khl*) plane, K is the Scherrer constant= 0.89-0.94, λ is wavelength of the X-ray beam used (1.541 Å or 0.154 nm), β_{khl} is the Full width at half maximum (FWHM) of the peak in radiance if ZnO crystal assumed to be spherical (β = (FWHM × 3.14/180)) and θ is the Bragg angle.

2.4.2. BET total surface area

BET total surface area of the prepared samples was determined by the analysis of N_2 adsorption isotherms at -196ºC using an automatic volumetric apparatus (Quantachrome TouchWin™ Automated Gas Sorption system version 1.21).

2.4.3. Energy dispersive X-ray spectroscopy

Energy dispersive X-ray spectroscopy (EDX) was obtained to characterize element content of the sample. EDX was measured using electron backscatter diffraction (FEI Quanta FEG-250, EDX).

2.4.4 Scanning electron microscope

The surface morphology of the obtained samples was determined using field-emission scanning electron microscope (FEI-SEM, Quanta FEG-250).

2.4.5. Fourier transforms infrared

Fourier transforms infrared (FTIR) spectroscopy to give the main functional groups on the obtained samples was done using a KBr disk technique and FTIR 6500 spectrometer (JASCO, Japan) in the range of 400-4000 cm^{-1}.

2.4.6. UV-Vis Diffuse Reflectance Spectroscopy (DRS)

UV–Vis diffuse reflectance spectra were measured on a UV–Vis/NIR spectrophotometer (JASCO Corp., V-570, UK) with wavelength range of 190 – 2500 nm was performed to estimate the band-gap energy (E_g, eV) of each sample.

2.5. Photochemical experiments

The photocatalytic performance of each sample was tested toward degradation of a cationic dye such as methylene blue (MB) under both dark and sunlight as visible light irradiation. The photodegradation experiments of methylene blue dye (MB) were run under sunlight irradiation at interval times between 0-180 min. Prior to the visible irradiation, the solid photocatalyst sample and MB dye solution mixture were stirred in the dark for 30 min at 25ºC to attain the adsorption-desorption equilibrium and ensure that the removal of dye was completed by the photocatalytic process. All photo experiments were carried out at working pH of MB dye which is equal to 6. This is suitable pH to prevent the dissolution of ZnO which happens in acidic media.

About 0.1g photocatalyst was put into the 50 ml MB solution (10 mg/L) and pH was fixed at neutral media ~ 6. Then, the mixture was vigorously stirred for 30 min in a dark environment to attain the adsorption equilibrium of the sample. Then the photocatalytic degradation was monitored by measuring the absorbance of MB solution every 10 min or 30 min using the ultraviolet–visible spectrophotometer (Shimadzu-PC2401) at its λ_{max} value (664 nm). In order to assess the reproducibility and error of adsorption and photodegradation tests, the absorbance of dye was recorded three times to take the average value.

The removal efficiency (% R) of MB dye was calculated using the following equation:

$$\% R = \frac{(C_0 - C_t)\ 100}{C_0} \quad (2)$$

where C_0 and C_t are the liquid-phase concentrations of dye in an aqueous solution (mg/L) at initial and equilibrium time (min), respectively.

3. Results and discussion

3.1. Crystal features of prepared catalysts

The phase characteristics of pure ZnO, 40%C-N/ZnO (N_2)and 40%N/ZnO (air) samples were obtained using XRD analysis. Fig. 1 depicts the comparison between XRD patterns for ZnO before and after doping with C-N and N at 40wt% of urea which calcined with zinc acetate at 500ºC for 2h in either nitrogen or air atmosphere. Notably, All XRD profiles showed the corresponding nine characteristic diffraction patterns of ZnO before and after doping. It can be seen that all doped ZnO samples present similar diffraction peaks to that of pure ZnO of (100), (002), (101), (102), (110), (103), (200), (112) and (201) located at 2θ= 31.8º, 34.4º, 36.2º, 47.5º, 56.5º, 62.8º, 66.3º, 67.9º and 69.0º according to JCPDS# 36-1451 [18-25]. The obtained crystallite sizes of pure ZnO are varied between 15.5 and 45.8 nm with average size of 27.4 nm. Incorporation of C and/or N upon calcination at air causes slight shifting of 2θ to lower values with a slight increase in d-spacing followed by a higher reduction in the intensity than that happened upon calcination under nitrogen atmosphere. However, there were no additional peaks of N or C elements and thus pure ZnO with a hexagonal structure was obtained and good crystallinity. However, the 40%C-N/ZnO (N_2) catalyst has more crystallinity than that 40%N/ZnO (air) catalyst. This is indicated also by the

crystallite size value of prepared catalysts where the crystallite sizes of 40%C-N/ZnO (N_2) varied from 16.5 to 43.4 nm, and from 7.02 to 27.8 nm for40%N/ZnO (air). Analogous findings were reported by previous investigators [18-25]. After doping with N, the peaks were broadened and their intensities were lowered. These are most likely due to a crystallinity decrease as a result of crystal growth inhibition by the urea due to the substitution of O by N [32].Therefore, there is a substitution for oxygen sites on ZnO by either C or N atom which can enter the interior of the crystal lattice of ZnO and replaces O in C-N/ZnO (N_2) sample because of the ionic radii of O and N are almost the same [19].

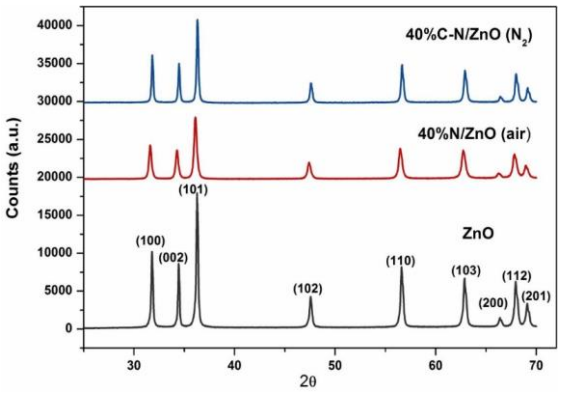

Fig. 1: XRD patterns of bare ZnO, 40%N/ZnO (air) and 40%C-N/ZnO (N_2) samples.

3.2. Surface area, composition and morphology characteristics

The specific total surface areas (S_{BET}, m^2/g) are given in Table 1. The specific surface area varied from 37.9 to 57.4 m^2/g. A maximum value was observed on 40% N-doped ZnO (air). Upon co-doping, the total specific surface area was slightly reduced to 30.8 m^2/g. Thus, 40% N-doped ZnO (air) exhibits higher S_{BET}, m^2/g than the value of pure ZnO by an enhancement of 34%, indicating that air calcination plays an important role by introducing the nitrogen into ZnO matrix and facilitating the formation of ZnO particles with porous surfaces as a result of breakdown carbon atoms also. As listed in Table 1, the EDX analysis confirmed the formation of ZnO with purity reached to 100% (84.1%Zn and 15.9%O). Co-doping with C and N yielded ZnO with high content of C (23.5%) and low content of N (1.9%), otherwise, 40%N-ZnO has high content of N (12.7%) and carbon is not detected. From these results, we can conclude that the ZnO is successfully doped through mono- and bi-nonmetals.

Scanning electron microscope (SEM) images of the selected samples for exploring their surface morphologies before and after doping are depicted in Fig. 2. It has been observed in SEM image of ZnO pure that the surface has somewhat short hexagonal rods shaped particles besides Zn particles in irregular sphere-shapes as accord with the SEM results obtained by Bouarroudj et al. [17]. However, the particles size distribution of spherical particles seems to be varied between 46 and 77 nm. This result is consistent with that obtained in XRD analysis of ZnO.

Table 1: Specific surface area, bandgap, average crystallite size from XRD and EDX analysis of the prepared samples.

Samples	S_{BET} (m^2/g)	Bandgap eV	Average crystallite size (nm)	EDX analysis (wt%)			
				Zn	O	C	N
ZnO	37.9	3.07	27.39	84.1	15.9	0	0
40% C-N/ZnO(N_2)	30.8	2.97	28.17	52.5	22.1	23.5	1.9
40% N/ZnO (air)	57.4	2.83	18.98	60.5	26.8	0	12.7

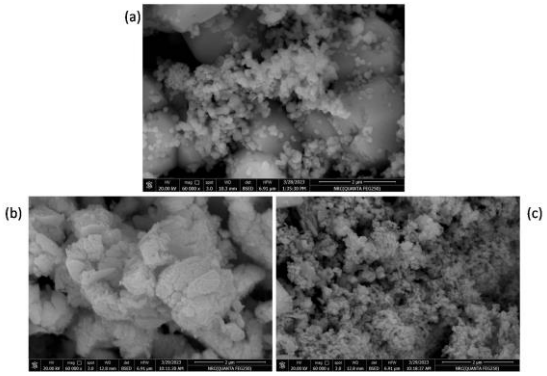

Fig. 2: SEM images of (a) Pure ZnO, (b) 40%C-N/ZnO (N2) and (c) 40%N/ZnO(air) samples.

The SEM morphology of ZnO after doping with 40%C-N/ZnO showed a multilayer of C particles covering the ZnO surface, while no comparable changes occurred for 40%N/ZnO sample which containing spherical particles of ZnO with low aggregation action when N element incorporated into ZnO matrix.

3.3. Surface functional groups investigation

The functional groups of ZnO NPs and their doped samples were identified using FTIR analysis in the range of 4000 to 400 cm−1 as illustrated in Fig. 3. As observed in all spectra, characteristic absorption bands of O–H group stretching and bending vibration modes of water molecule physiosorbed on ZnO surface can be observed at 3422 and 1630 cm−1 [18-25], respectively. An extended broad band at 1123cm-1which split into two small peaks at 1109 cm-1 and 1048 cm-1 after doping, were assigned to the symmetric stretching vibration of O–C=O and–C–O groups respectively. Characteristic absorption bands

related to Zn–O stretching and bending vibration modes are appeared at around 616 cm-1 and 486 cm-1 for pure ZnO, respectively; and then shifted to 470–459cm-1 with broadening and increasing in their absorption frequency when ZnO doped with the nonmetals, confirming the formation of C,N–O–Zn. However, it was observed presently a difference is that the intensity of the absorption bands for O-H, O–C=O and–C–O are increased frequently after doping. This behavior can be ascribed to the variation of the oxygen defect density [19, 21].

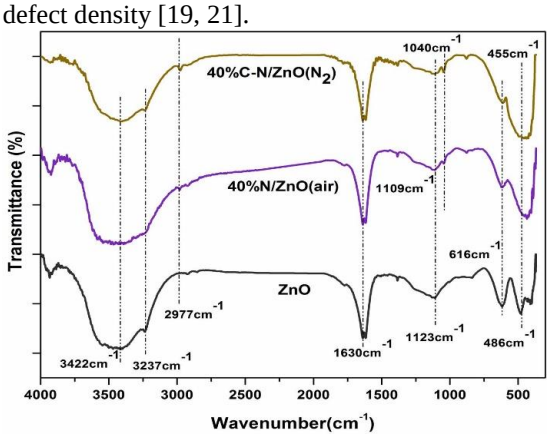

Fig. 3: FTIR spectra of ZnO, 40%N/ZnO (air) and 40%C-N/ZnO samples.

3.4. Bandgap estimation of as-prepared catalysts

The absorption properties of samples were investigated via the UV–vis DRS spectra as depicted in Fig. 4 for pure ZnO and their corresponded doped with nonmetals. The calculated bandgap values are listed in Table 1.UV-Vis-NIR spectroscopy proved that the absorbance of the 40%N/ZnO(air) in the visible and infrared region is considerably higher than that of 40%C-N/ZnO and undoped ZnO. This result results indicated that e−– h+ pairs recombination was inhibited once N was included in the ZnO material [21]. The calculated energy bandgap values in Table 1indicated that the sequence ordering of the corresponding as-prepared catalysts was found in the following tendency:40%N/ZnO(air)>40%C-N/ZnO>ZnO. It can be concluded that the obtained doped catalysts shall be improved the sunlight photocatalytic system used in this study.

3.5. Photoactivity evaluation of ZnO doped with mono-nonmetals

The synthesis of ZnO doped with nitrogen as mono-nonmetal with ZnO was studied at varying concentrations of 5 to 40 wt% for measuring the photocatalytic activity. Since reactants, e.g., zinc acetate as a zinc source and urea used as a source of nitrogen and carbon elements, are containing higher content of carbon elements, the calcination was performed at 500oC for 2h under air atmosphere inside a muffle furnace. The prepared samples were noted as 5%N/ZnO, 15%N/ZnO, 25%N/ZnO and 40%N/ZnO. Their photodegradation abilities are shown in Fig. 5 as a relationship between interval times (min) against photodegradation % of MB dye in the aqueous solution. Pure ZnO exhibited about 50, 65 and 100% photodegradation of MB dye at 30, 60 and 180 min, respectively. It was observed that increasing the concentration of N dopant from 5 to 40%, the photodegradation of MB dye increases from 68.1 to 83.7% and from 90.9 to 100% gradually, at 30 and 60 min, respectively. As a result, the complete degradation of MB dye was obtained at 60 min when contacted with 40%N/ZnO which has bandgap of 2.83eV (*cf.* Table 1).

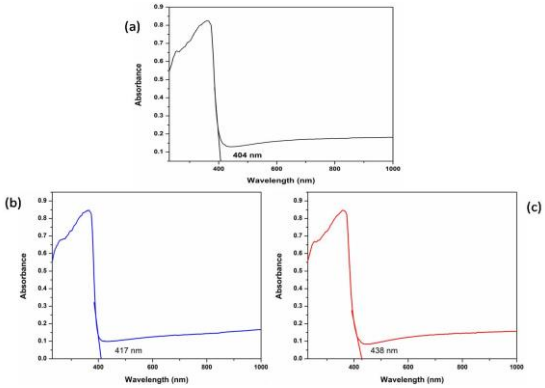

Fig. 4 : UV–vis DRS spectra of (a) ZnO pure, (b) 40%C-N/ZnO(N2) and (c) 40%N/ZnO(air) samples.

However, all doped photocatalysts showed 100% degradation of MB dye after 120 min. Thereof, N-doped ZnO photocatalysts were found to exhibit enhanced photocatalytic degradation for MB dye under sunlight irradiation in comparison with the undoped ZnO.

It is reported that the N atoms doping effectively improves the light absorption of ZnO in the visible range [33]. Klingshirn et al. [34] have proved that N impurities act as superficial acceptors in ZnO crystals. This is due to the improvement of bandgap and total specific surface area in the N-doped ZnO which can suppress the recombination of the photogenerated electron-hole pairs [35]. Plausible mechanism of photocatalytic degradation of MB dye by N/ZnO with the sunlight irradiation is including the next steps: During the sunlight irradiation, the N/ZnO photocatalyst can easily absorb the light energy to create the conduction band electrons (eCB−) and valence band holes (hVB+) [36]. Then, the photoexcited eCB− interacts with dissolved oxygen (O2) to generate a superoxide radical (O2•−) [37]. Besides, the photogenerated hVB+ can directly oxidize the MB dye to form degradation products or can react with the water (H2O) to produce the hydroxide radical (•OH) [36, 38]. Both radicals of O2•− and •OH are shown to be good oxidizing agents

that readily attack MB dye molecules to produce end products of CO_2 and H_2O.

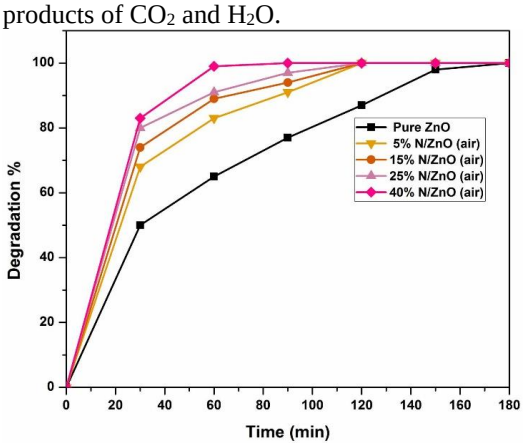

Fig. 5: Photodegradation of MB dye using pure ZnO and N-doped ZnO samples during sunlight irradiation [MB concentration = 10mg/L, catalyst dose = 0.1g/50mL, pH = 6].

3.6. Photoactivity evaluation of ZnO doped with bi-nonmetals

Upon on calcination of zinc acetate with different ratios of urea (i.e., 5, 15, 25 and 40%) at 500oC for 2h under nitrogen flow, carbon-nitrogen (C-N) co-doped ZnO photocatalysts were prepared. The photocatalytic activity of these materials was determined through sunlight irradiation of MB dye at different times as depicted in Fig. 6. It was indicated that the increase in the concentration yield of C-N in the ZnO crystals from 5 to 40% increases the photodegradation of MB dye from 58.9 to 79.1% and about 89.0 to 100% gradually, at 30 and 90 min, respectively. By comparing these values with earlier N-doped ZnO samples, the photoactivity of N-ZnO is found to be higher than that of C-N/ZnO. This result is owing to the smaller bandgap (i.e., 2.83 eV for 40%N/ZnO and 2.97 eV for 40%C-N/ZnO, Table 3.3) and the higher total specific surface area of N-ZnO photocatalyst (i.e., 57.4 m2/g for 40%N/ZnO and 30.8 m2/g for 40%C-N/ZnO, Table 1). At 120 min, all MB dye molecules were breakdown fully by 5%,15% and 25% C-N/ZnO photocatalysts. Thus, a superior photocatalytic activity for N-doped ZnO is achieved as a result of enhanced absorption capacity and extended light-response region.

3.7. FTIR investigation of catalysts after photodegradation

To verify the occurrence of adsorption and photodegradation of MB dye, the surface functional groups of the prepared catalysts before and after photodegradation of MB dye were determined using FTIR tool and represented in Fig.7. It was found that there is a big difference in photocatalytic behavior between FTIR spectrum of ZnO and that of other doped samples after photodegradation. For ZnO, there is a reduction in all absorption peaks which related to functional groups O–H, O=C–O, and Zn–O. This result can be concerned to the adsorption of MB dye onto ZnO surface [39].

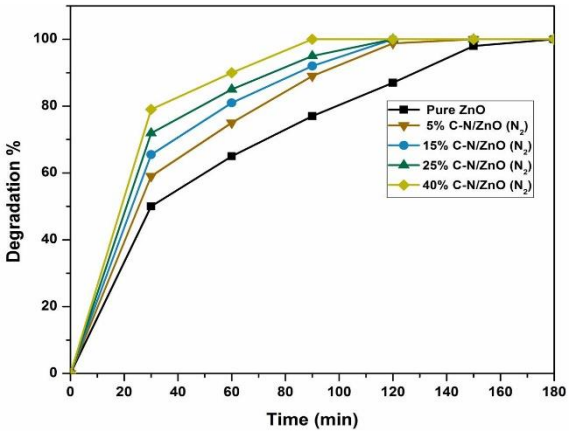

Fig. 6: Photodegradation of MB dye using pure ZnO and N-doped ZnO samples during sunlight irradiation [MB concentration = 10mg/L, catalyst dose = 0.1g/50mL, pH = 6].

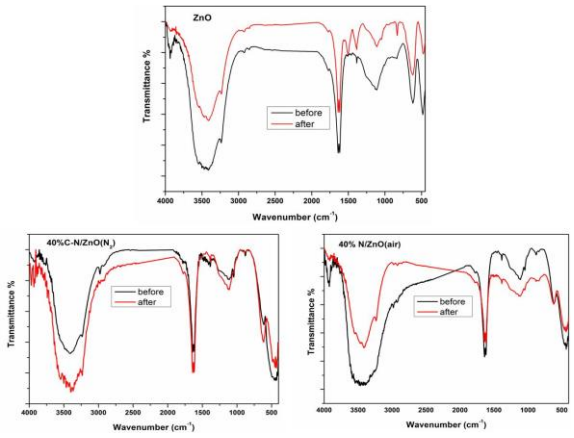

Fig. 7: FTIR spectra of the prepared catalysts before and after the photodegradation run of MB dye from aqueous solutions during sunlight irradiation [dye concentration = 10mg/L, catalyst dose = 0.1g/50mL, pH = 6].

Upon photodegradation of MB dye by ZnO doped with 40% C-N, the intensity of absorption bands for O–H, and O=C–O groups is increased while that for Zn–O group vibration band is decreased. However, photodegradation of MB dye decreased the absorption bands related to O–H, and Zn–O but increased the absorption band of O=C–O groups in the case of 40%N/ZnO sample. Enhancement in the absorption bands intensity of O–H and O=C–O groups may be attributed to the formation of H2O and CO2 products of the photodegradation process of MB dye by the prepared samples under sunlight irradiation.

4. Conclusions

ZnO nanoparticles and their doped samples with nonmetals such as N and C have been successfully prepared using sol-gel method and then calcined in either air or nitrogen atmosphere. The prepared samples were characterized by XRD, SEM, EDX, FTIR, BET surface area and UV-vis DRS analyses. The XRD results showed a distinct decrease in the crystallinity of doped samples especially the sample that was calcined in air atmosphere (N-ZnO). Also, the specific surface area of (N-ZnO) was the highest value which agrees with XRD results. Thus, 40%N/ZnO sample showed the superior photocatalytic activity as a result of enhanced absorption capacity and extended light-response region. Therefore, the modification of ZnO with doping by nonmetals could decrease the recombination time of photo-induced charged electrons and holes which is a necessary process for enhancing the photocatalysis of ZnO.

Acknowledgment

Authors are thankful to the National Research Center, Egypt for supporting this work with technical facilities including chemicals and equipments.

Author's Declaration

Compliance with ethical standards

Financial Disclosure statement

The author(s) received no specific financial funding for this work.

Conflict of interest

The authors declare that they have no known competing financial interests or personal relationships that could have appeared to influence the work reported in this paper.

References

1- M. Hasanpour, M. Hatami, Photocatalytic performance of aerogels for organic dyes removal from wastewaters: Review study, Journal of Molecular Liquids 309, 113094 (2020).

2- N. B. Singh, G. Nagpal, S. Agrawal, Water purification by using adsorbents: a review, Environmental technology & innovation 11, 187-240 (2018).

3- V.K. Gupta, R. Kumar, A. Nayak, T. A. Saleh, M.A. Barakat, Adsorptive removal of dyes from aqueous solution onto carbon nanotubes: a review, Adv. Coll. Interf. Sci. 193, 24-34 (2013).

4- V. Katheresan, J. Kansedo, S.Y. Lau, Efficiency of various recent wastewater dye removal methods: A review, J. Environ. Chem. Eng. 6, 4676-4697 (2018).

5- J. F. García-Araya, F. J. Beltrán, Photocatalytic oxidation/ozonation processes, Catalysts 13, 314 (2023).

6- Y. Mao, Y. Li, Y. Zou, X. Shen, L. Zhu, G. Liao, Solvothermal synthesis and photocatalytic properties of ZnO micro/nanostructures, Ceram. Inter. 45, 1724-1729(2019).

7- X. Yang, Y. Yang, B. Wang, T. Wang, Y. Wang, D. Meng, Synthesis and photocatalytic property of cubic phase CdS, Solid State Sci. 92, 31-35 (2019).

8- A. Kusior, K. Michalec, P. Jelen, M. Radecka, Shaped Fe2O3 nanoparticles–synthesis and enhanced photocatalytic degradation towards RhB, Appl. Surf. Sci. 476, 342-352 (2019).

9-W.S. El-Yazeed, A.I. Ahmed, Photocatalytic activity of mesoporous WO3/TiO2 nanocomposites for the photodegradation of methylene blue, Inorg. Chem. Comm. 105, 102-111(2019).

10- R. J. Barnes, R. Molina, J. Xu, P. J. Dobson, I. P. Thompson, Comparison of TiO2 and ZnO nanoparticles for photocatalytic degradation of methylene blue and the correlated inactivation of gram-positive and gram-negative bacteria, J. Nanoparticle Res. 15, 1432 (2013).

11-A. Di Mauro, M. E. Fragalà, V. Privitera, G. Impellizzeri, ZnO for application in photocatalysis: From thin films to nanostructures, Mater. Sci. Semico. Process. 69, 44–51 (2017).

12- K. M. Lee, C. W. Lai, K. S. Ngai, J. C. Juan, Recent developments of zinc oxide based photocatalyst in water treatment technology: A review, Water Res. 88, 428–448 (2016).

13- N. Güy, M. Ozacar, The influence of noble metals on photocatalytic activity of ZnO for Congo red degradation, Int. J. Hydrogen Energy 44 (41), 20100–20112 (2016).

14- Z.Y. Wang, B.B. Huang, Y. Dai, X.Y. Qin, X.Y. Zhang, P. Wang, H.X. Liu, J.X. Yu, Highly photocatalytic ZnO/In2O3 heteronanostructures synthesized by a coprecipitation method, J. Phys. Chem. C 11 (113), 4612–4617 (2014).

15- S.W. Zhao, H.F. Zuo, Y.R. Guo, Q.J. Pan, Carbon-doped ZnO aided by carboxymethyl cellulose: fabrication, photoluminescence and photocatalytic applications, J. Alloys Compd. 695, 1029–1037(2017).

16- B.M. Rajbongshi, S.K. Samdarshi, ZnO and Co-ZnO nanorods-complementary role of oxygen vacancy in photocatalytic activity of under UV and visible radiation flux, Mater. Sci. Eng., B 182, 21–28 (2014).

17- T. Bouarroudj, L. Aoudjit, L. Djahida, B. Zaidi, M. Ouraghi, D. Zioui, S. Mahidine, C. Shekhar, K.Bachari, Photodegradation of tartrazine dye favored by natural sunlight on pure and (Ce, Ag) co-doped ZnO catalysts, Water Sci. Technol. 83, 2118–2134 (2021).

18- A.B. Lavand, Y.S. Malghe, Synthesis, characterization and visible light photocatalytic activity of nitrogen-doped zinc oxide

nanospheres, J. Asian Ceramic Societies 3, 305-310 (2015).
19. C. Tang, C. Chen, H. Zhang, J. Zhang, Z. Li, Enhancement of degradation for nitrogen doped zinc oxide to degrade methylene blue, Physica B 583 412029 (2020).
20- R. Kabir, Md. Abu Khalid Saifullah, A.Z. Ahmed, S. Md. Masum, Md. Ashraful Islam Molla, Synthesis of N-doped ZnO nanocomposites for sunlight photocatalytic degradation of textile dye pollutants, J. Compos. Sci. 4, doi:10.3390/jcs4020049, (2020).
21- J. J. Macías-Sánchez, L. Hinojosa-Reyes, A. Caballero-Quintero, W. de la Cruz, E. Ruiz-Ruiz, A. Hernández-Ramírez , J. L. Guzmán-Mar, Synthesis of nitrogen-doped ZnO by sol–gel method: characterization and its application on visible photocatalytic degradation of 2,4-D and picloram herbicides, Photochem. Photobiol. Sci, doi: 10.1039/c4pp00273c.1-7, (2014).
22- A.B. Kumar, S. Billa, E.G. Shankar, M. C. S. Subha, C, N dual-doped ZnO nanofoams: a potential antimicrobial agent, an efficient visible light photocatalyst and SXAS studies, J. Synchrotron Rad. 27, 90–99 (2020).
23- O. Haibo, H.J. Feng, L. Cuiyan, C. Liyun, F. Jie, Synthesis of carbon doped ZnO with a porous structure and its solar-light photocatalytic properties, Mater. Lett. 111, 217–220 (2013).
24- A.B. Lavand, Y.S. Malghe, Synthesis, characterization and investigation of visible light photocatalytic activity of C, N co-doped ZnO, Adv. Mater. Lett. 7(3), 181-186 (2016).
25- V. Kumari, A. Mittal, J. Jindal, S. Yadav, N. Kumar, S-, N- and C-doped ZnO as semiconductor photocatalysts: a review, Front Mater Sci 13, doi. org/ 10. 1007/ s11706- 019-0453-4, (2019).
26- H. Qin, W. Li, Y. Xia, T. He, Photocatalytic activity of heterostructures based on ZnO and N-doped ZnO, ACS Appl. Mater. Interf. 3, 152–3156 (2011).
27- U.K. Gautam, L. Panchakarla, B. Dierre, X. Fang, Y. Bando, T. Sekiguchi, A. Govindaraj, D. Golberg, C. Rao, Solvothermal synthesis, cathodoluminescence, and field- emission properties of pure and N- doped ZnO nanobullets. Adv. Funct. Mater. 19, 131–140 (2009).
28- A.P.Bhirud, S.D. Sathaye, R.P. Waichal, L.K. Nikam, B.B. Kale, An eco-friendly, highly stable and efficient nanostructured p-type N-doped ZnO photocatalyst for environmentally benign solar hydrogen production, Green Chem. 14, 2790–2798 (2012).
29- C.L. Perkins, S.-H. Lee, X. Li, S.E. Asher, T.J. Coutts, Identification of nitrogen chemical states in N-doped ZnO via X-ray photoelectron spectroscopy, J. Appl. Phys. 97, 034907 (2005).
30- M.A.I.Molla, M. Furukawa, I. Tateishi, H. Katsumata, S. Kaneco, Fabrication of Ag-doped ZnO by mechanochemical combustion method and their application into photocatalytic Famotidine degradation. J. Environ. Sci. Health Part A. 54, 914–923 (2019).
31- J. Lu, Q. Zhang, J. Wang, F. Saito, M. Uchida, Synthesis of N-doped ZnO by grinding and subsequent heating ZnO-urea mixture, Powder Technol. 162, 33–37 (2006).
32- H. Sudrajat, S. Babel, A novel visible light active N-doped ZnO for photocatalytic degradation of dyes, J. Water Proc. Eng. 16, 309–318 (2017).
33. W.L. Yu, J.F. Zhang, T.Y. Peng, New insight into the enhanced photocatalytic activity of N-, C- and S-doped ZnO photocatalysts. Appl. Catal. B,181, 220–227 (2016).
34. C.F. Klingshirn, ZnO: Material, physics and applications, Chem. Phys. Chem. 8,782–803 (2007).
35. S. Suna, X. Chang, X. Li, Z. Li, Synthesis of N-doped ZnO nanoparticles with improved photocatalytical activity. Ceram. Inter. 39, 5197–5203 (2013).
36. E. Prabakaran, K. Pillay, Synthesis of N-doped ZnO nanoparticles with cabbage morphology as a catalyst for the efficient photocatalytic degradation of methylene blue under UV and visible light, RSC Adv. 9, 7509–7535 (2019).
37. M.A.I. Molla, M. Furukawa, I. Tateishi, H. Katsumata, T. Suzuki, S. Kaneco, Photocatalytic decolorization of dye with self–dye–sensitization under fluorescent light irradiation, Chem Eng. 1, 8 (2017).
38. Y. He, Y. Wang, L. Zhang, B. Teng, M. Fan, High-efficiencyconversion of CO2 to fuel over ZnO/g-C3N4 photocatalyst, Appl. Catal. B. 168–169, 1–8 (2015).
39- X. Zhang, Y. Wang, F. Hou, H. Li, Y. Yang, X. Zhang, Y. Yang, Y. Wang, Effects of Ag loading on structural and photocatalytic properties of flower-like ZnO microspheres, *Appl. Surf. Sci.* 391, 476–483 (2017).